Computer simulation of stress-strain states in zygomatic bones after complex installation of implants

Timur Dibirov, Aleksey Drobyshev, Eduard Kharazyan, Nikolay Redko, Egor Pankov
Maxillofacial Surgery Department, A.I. Yevdokimov Moscow State University of Medicine and Dentistry, Russia
rumit.05@mail.ru, https://orcid.org/0000-0003-0876-928X
dr.drobyshev@gmail.com, https://orcid.org/0000-0002-1710-6923
edwardkharazian@hotmail.com, https://orcid.org/0009-0008-6750-7080
dr.redko@mail.ru, http://orcid.org/0000-0001-7807-9351
pankov.doc@mail.ru, http://orcid.org/0000-0003-0234-554X

Alexander Kozulin
Department of Solid Mechanics, Physical-Technical Faculty of National Research Tomsk State University, Russia
kozulyn@ftf.tsu.ru, http://orcid.org/0000-0002-2345-6790

Sergey Panin
Laboratory of Mechanics of Polymer Composite Materials, Institute of Strength Physics and Materials Science of Siberian Branch of Russian Academy of Sciences, Tomsk, Russia
svp@ispms.ru, http://orcid.org/ 0000-0001-7623-7360

Sergey Arutyunov
Digital Dentistry Department, A.I. Yevdokimov Moscow State University of Medicine and Dentistry, Russia
sd.arutyunov@mail.ru, http://orcid.org/0000-0001-6512-8724

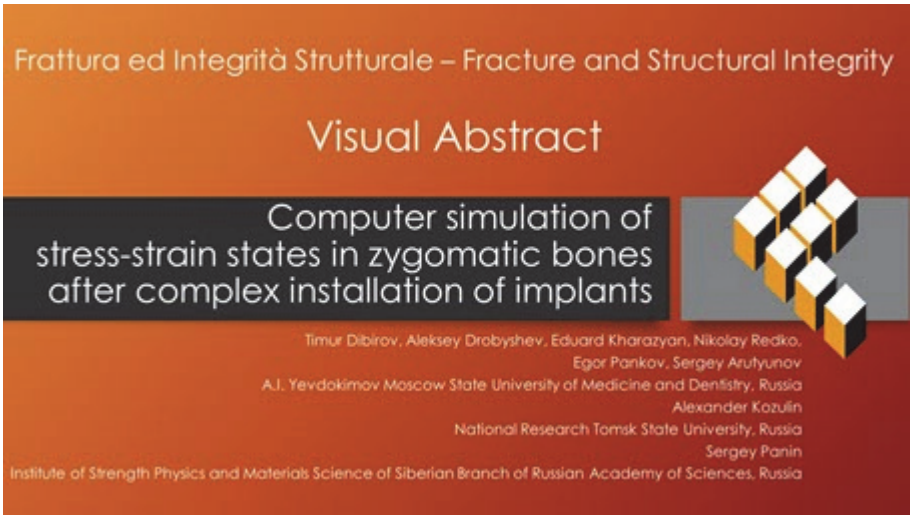

OPEN ACCESS

Citation: Dibirov, T., Drobyshev, A., Kharazyan, E., Redko, N., Pankov, E., Kozulin, A., Panin, S., Arutyunov, S., Computer simulation of stress-strain states in zygomatic bones after complex installation of implants, Frattura ed Integrità Strutturale, 67 (2024) 259-279.

Received: 12.10.2023
Accepted: 13.11.2023
Online first: 08.12.2023
Published: 01.01.2024

KEYWORDS. Zygomatic implant, Finite Element Method (FEM), Stress-Strain State (SSS), Failure, Denture base, Elastic Modulus.

INTRODUCTION

Despite the enormous efforts of the global medical community, the growing dynamics of the number of cancer diseases is accelerating nowadays. This trend is unlikely to change in the foreseeable future due to the aging population, regular stressful situations, as well as environmental, economic and other factors [1]. According to the International Agency for Research on Cancer (IARC), more than 18 million new cancer cases and above 9.5 thousand deaths it caused was recorded worldwide in 2018 [2]. Both head and neck cancers are among the most common types, ranking eighth as the leading cause of death [3]. In this regard, an improvement of methods of complex maxillofacial and orthopedic treatment is an urgent problem in medicine.

In general, the loss of bone tissue of the maxilla due to oncological or traumatic surgery is a serious medical and social challenge. Its advanced treatments are based on the installation of zygomatic implants that have been proposed by Prof. Bronemark in 1988 as a support for maxillary dentures [4]. Their first generation differed from up-to-date analogues only in greater both length and diameter.

Currently, zygomatic implants are produced in a wide range of standard sizes, but the selection of their types, quantity and configuration is an exclusively patient-oriented problem [5-7]. It is also associated with the presence/absence of bone tissue in one or another section of the zygomatic bones, its condition, and some other issues [8, 9]. In particular, an analysis of bone optical density is typically carried out on the basis of cone beam computed tomography (CBCT) according to the Mish classification [10]. For this purpose, the main estimated values of X-ray bone tissue density were implemented using the Hounsfield scale (HU) [11]: a healthy bone (D1) at ≥850 HU; a pastous bone (D2) at 350–850 HU; and a bone affected by local osteoporosis (D3) at ≤350 HU. However, in spite of manufacturers' recommendations for the use of a specific type of zygomatic implants depending on the presence and condition of bone tissue, the selection of their number and configuration is made intuitively in most cases, taking into account the experience of maxillofacial surgeons [12, 13].

When installing zygomatic implants, an important aspect is to predict their mechanical behavior in addition to some other biomedical issues (primarily, osseointegration). The problem of assessing the deformation behavior of the "zygomatic bones–implants–maxillary prosthesis" system (prosthetic structure) can be solved within the framework of solid mechanics approaches, but the structure itself can be approximated by the finite element method (FEM). In this formulation, the solution to the problem of selecting the type, configuration and location of installed zygomatic implants can be carried out when planning prosthetic tactics based on the results of computer simulation [14–16]. In this case, information about the skull of a particular patient, and the zygomatic bones as its components, can be taken from computed tomography (CT) data and imported into commercial FEM-based software packages then. Certainly, such activities i) increase the efficiency of treatment of these severe dental diseases, ii) reduce the risk of medical errors and possible postoperative complications [17].

Since experimental methods do not enable to clearly determine the patterns of biomechanical processes of interaction between bone tissue and implants, the FEM-based computer simulation is most often used for such qualitative analyzes, since it is characterized by the most advanced algorithms. Its advances by the possibility to study the initiation and development of mechanical effects around implants, reducing the time and cost of research for planning their installation.

Nevertheless, it is often not possible to validate the results of computer simulation and verify them with experimental data in biomechanics (even when studying biological bone tissue). In addition, computer simulation cannot fully reproduce the human body conditions [18–20]. As a result, some simplifications are required in developing adequate models. In this study, the implementation of the FEM was motivated by the lack of a sufficient set of verified experimental data in the field of dental implant surgery. For this reason, the results of computer simulation can be considered prognostic and used when planning complex operations by changing the control parameters of the models. This enables to compare the data obtained by going through hundreds of possible options with the optimal clinical treatment (surgical effects).

Before formulating the research problem, it is appropriate to mention the main factors influencing the pattern of the stress-strain state (SSS) in the zygomatic bones with installed zygomatic implant:

- bone density at their attachment areas;
- their standard sizes (primarily in terms of length);
- symmetry of the zygomatic bones of a skull, including their dimensions and shapes;

- possible local absence of bone tissue fragments due to previous surgery resection.

The aim of this research was to evaluate the SSS in the "zygomatic bones–implants–denture base" system by varying the type and number of the implants, as well as applying loads. The system was loaded locally, affecting segments of a virtual denture base of a maxillary prosthesis (hereinafter referred to as the denture base). The load magnitude was varied over a wide range, characteristic of the mastication process [21]. Using the only denture base in computer simulation was a certain approximation, which enabled to exclude the influence of the shape (curvature) of the mastication surface and the size of the installed dentition on the results of the SSS calculations. However, its functional purpose in terms of consolidating the abutments with the denture base was identical to the entire maxillary prosthesis.

The paper is compiled as follows. Section 2 describes materials and research methods, as well as some features of the FEM-based computer simulation. In addition, it introduces a critical state criterion, reports some details of developing numerical models, importing CT data, and installing of virtual zygomatic implants into a digital model of a skull (including zygomatic bones). Subsection 3.1 presents the results of the SSS calculations for the "Zygan implant (top row)–Oncology implant (bottom row)" configuration without a denture base. Subsection 3.2 shows similar data for the "zygomatic bones–implants–denture base" system when varying both location and magnitude of applied loads. Subsection 3.3 is devoted to variation of the load direction relative to the denture base. Preceding conclusions, an algorithm for solving the problem of the installation of zygomatic implants by computer simulation was proposed in Section 4 as a discussion point.

MATERIALS AND METHODS

At the first stage of the study, a 3D digital model of a human skull was developed for the SSS calculations according to the reverse engineering concept. It was appropriate for the FEM-based computer simulation, widely implemented for many engineering applications. The model was developed in several stages using CT data (Philips Diamond Select Brilliance CT 64-slice) of a particular patient. It maximally reflected the pronounced structural features, including those arising as a result of bone tissue resection. The CT data in DICOM format were processed by the Invesalius® software package [22]. In this case, the bone tissue of the skull was isolated and visualized from the entire data array. Then, its 3D reconstruction was saved in the "*.stl" format for export to computer-aided design (CAD) software.

The stage of final processing of the solid model in the CAD format, including its preparation for a FEM analysis (Fig. 1, a), consisted of eliminating artifacts and small pores [23] of the tomographic model and simplifying the shape of the studied skull segments. It was assumed that a load applied to implants would form (transmit) an SSS in the zygomatic bones of the anterior-facial part of the skull. For this reason, the facial part of the skull, containing both frontal and zygomatic bones, was visualized (Fig. 1, b). The process was based on the shape idealization principles to simplify the solution and to analyze the results.

An additional challenge for the prostheses' installation was a lesion of the left zygomatic bone, which, in fact, disrupted its connection with the bridge of the nose (shown as an oval in Fig. 1, b, presenting the digital model of the skull after removing artifacts and smoothing). In this case, the cartilage tissue and the bones of nose and palate, as well as the alveolar ridge were absent. Then, holes were numerically "drilled" in the zygomatic bones of the "improved" model of the skull for installing titanium implants. According to the basic requirements of the operation protocol, the installation must be carried out at a strict inclination angle and it was unacceptable to remove the implant abutments into the orbit or infratemporal fossa (Fig. 1, b). Subsequently, the model was used for computer simulation, but the denture base was additionally attached to the implants in this case (Fig. 1, d). In real conditions, a complete maxillary prosthesis would be installed instead (Fig. 1, c).

Two types of zygomatic implant models were applied (Fig. 1, d). The top row consisted of two Zygan implants 47.5 mm long with a diameter of both main and thread (contacting with the bone) parts of 3.4 mm. As the bottom row, two Oncology implants (ONC-55) were installed with a length of 37.5 mm. Their diameters were 3.5 and 4.1 mm for the main and thread parts, respectively. The minimum depth of the installation of the implants into the zygomatic bones was 15 mm (Fig. 1, b, c and d). The ratio of implant-to-(cylinder shaped) hole diameter was set as 1:1. The model did not employ the condition of bearing preload between the implant and bone tissue.

To calculate the SSS parameters in the skull bones and the zygomatic implants under the effect of physiological loads, the ANSYS Workbench® commercial software package was implemented. The calculation was carried out in the 3D statement and the static formulation of the load application. The problem was solved in the linear elastic statement, using a system of equations of solid mechanics, consisting of equilibrium Eqns. (1), as well as geometric Cauchy (2) and constitutive Hooke (3) relations. The presented system of equations with boundary conditions (4–7) was solved numerically by the FEM in the 3D formulation using tetrahedral elements in a computational mesh.

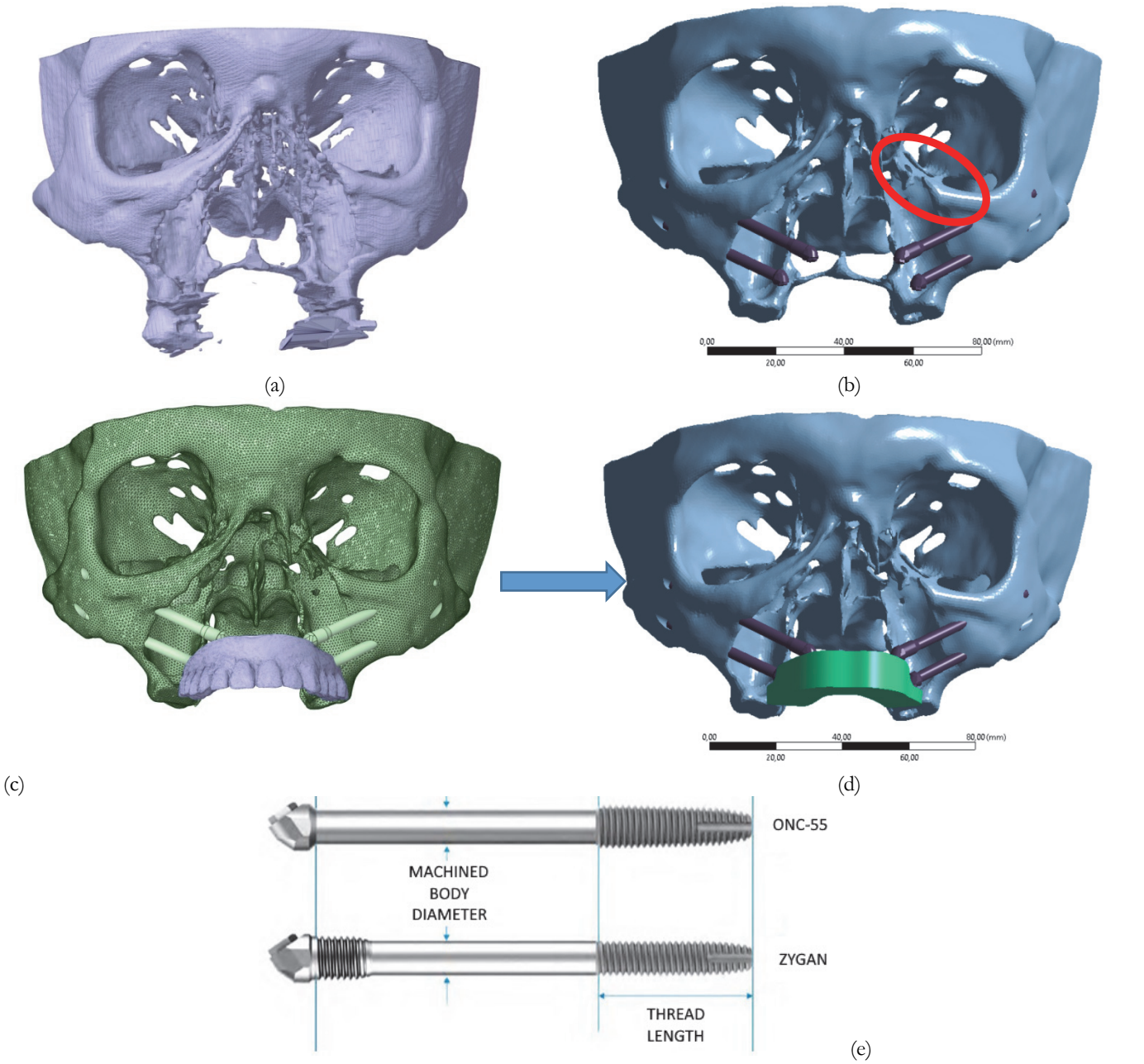

Figure 1: The virtual (digital) model developed using the CT data of the skull (a) and the "improved" one (b) indicating the location of the zygomatic implants; the same model with the maxillary prosthesis (c) and the denture base replacing it in the SSS calculations (d); a general view of the zygomatic implants (e).

$$\sigma_{ij,j} = 0 \tag{1}$$

$$\varepsilon_{ij} = \frac{1}{2}\left(u_{i,j} + u_{j,i}\right) \tag{2}$$

$$\sigma_{ij} = \lambda\theta\delta_{ij} + 2\mu\varepsilon_{ij} \tag{3}$$

where σ_{ij} and ε_{ij} were the stress and strain tensor components, respectively; u_i and u_j were the displacement vector components; δ was the Kronecker delta; $\theta = \varepsilon_{11} + \varepsilon_{22} + \varepsilon_{33}$ was volumetric strain; $\lambda = \dfrac{\nu E}{(1+\nu)(1-2\nu)}$ was Lamé's first parameter, $\mu = \dfrac{E}{2(1+\nu)}$ was shear modulus; ν, E were Poisson's ratio and Young's modulus (Tab. 1). The comma before the index meant differentiation by spatial coordinate.

The final mesh density as well as the average mesh size was selected based on the convergence of the computational experiment results. For two calculation cases, 3D models are shown in Fig. 2.

Boundary conditions were set as follows. The kinematic boundary conditions were the same for all calculations, namely rigid fixation along the surface A (Fig. 2, a):

$$u_x\big|_A = 0,\ u_y\big|_A = 0,\quad u_z\big|_A = 0 \tag{4}$$

The load boundary conditions were its vertical application to the abutments of each implant alternately for the *i* numbers of 1, 2, 3 and 4 according to Fig. 2, b for the first case of the calculations:

$$F_z(1) = F_i, \text{ where } F_i = 50 \text{ N}; \tag{5}$$

while such boundary conditions were in the form of a distributed compressive load applied orthogonally to the lower surface of the denture base alternately to the segments indicated in Fig. 2, c, simulating various options for redistributing the mastication load from the maxillary prosthesis in the second case:

$$F_z(2) = F_i \tag{6}$$

where F_i=50, 100, 150 N; *i* was the segment number of the lower surface of the denture base from 1 to 8, numbered from right to left, for the sequential application of the loads in the calculations.

For the third case, the load boundary conditions were in the form of a distributed compressive load applied at an α angle of 45° to the lower surface of the denture bases, first alternately but simultaneously then to segments 4 and 5 according to Fig. 2, c, simulating three options for loading the anterior teeth when biting:

$$F_z(3) = F_i\cos(\alpha),\ F_y(3) = F_i\cos(\alpha) \tag{7}$$

where F_i=50, 100, 150 N and *i*=4 and 5 were the load amplitude and the number of the loaded segments according to Fig. 2, c; α was the inclination angle.

In the contact area between the implants and the zygomatic bone, the contact boundary conditions provided for equality of displacements at the "implant–zygomatic bone" interface. In other words, the rigid fixation (ideal contact) conditions were implemented, implying successful osseointegration.

The use of the Ti-6Al-4V alloy, widely implemented for biomedical applications, was a topic discussion in recent years since its elastic modulus exceeded 100 GPa, i.e. it was mechanically incompatible (significantly superior) to that of bone tissue (5–30 GPa) [24]. This fact could provide the "stress shielding" phenomenon, which was observed when the implant absorbed applied loads and did not stimulate bone growth, enabling peri-implant bone resorption [25-30]. In addition, this led to fracture of natural bone tissue (aseptic loosening). However, this alloy (mainly with a protective coating deposited to prevent release of aluminum into a human body) is still a leader in the manufacturing medical implants, in particular those used in this study. Polymethyl methacrylate (PMMA) was selected as a material for prosthetic structures (denture base), products from which could be manufactured by 3D printing [31]. The skull bones possessed averaged parameters for a moderately mineralized aged state, with additional continuum averaging that did not take into account the distinction between cortical and trabecular parts. Values of the material properties of the model elements used in the calculations are presented in Tab. 1.

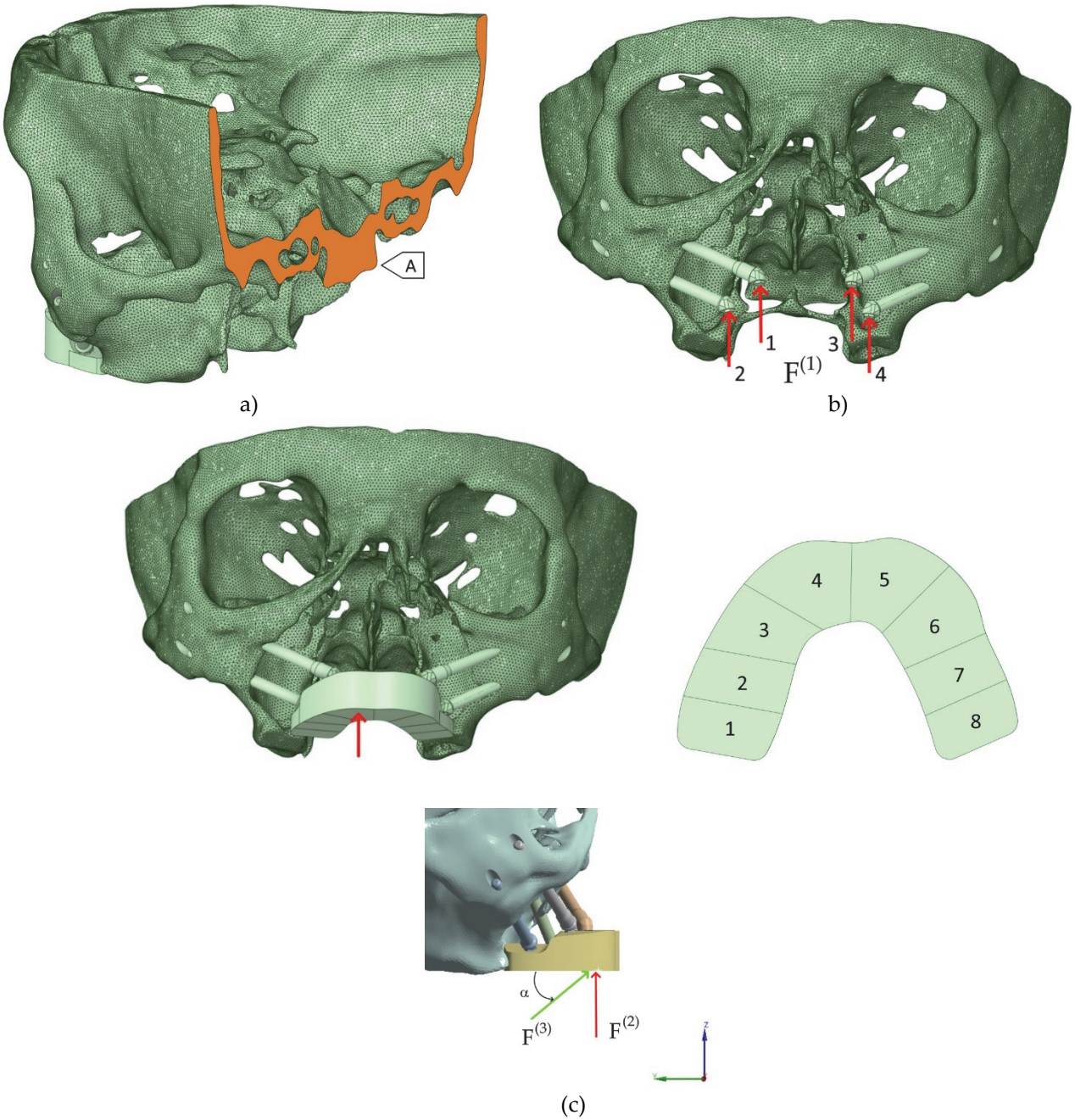

Figure 2: Schematic representation of boundary conditions for the 3D models: a) kinematic (rigid fixation along the surface A); b) loads on the implants (the calculation numbers); c) a schematic of the load application relative to the denture base.

Objects	E, GPa	υ	μ, GPa	K, GPa
Zygomatic bones	10.0	0.33	3.76	9.8
Virtual denture base	1.1	0.42	0.39	2.29
Titanium implants	96.0	0.36	35.00	114.00

Table 1: The mechanical properties of the materials used in the FE model.

For carrying out the strength analysis, some published data on the mechanical properties of bone tissue were used (Tab. 2) [32]. Note that generally accepted ideas about the averaged values of the mechanical properties of bone tissue were employed (in particular, cortical and trabecular ones), when choosing the values of permissible strength characteristics (for subsequent justification of the fracture/critical state criterion). The structure of bone tissue was determined by the resulting dynamic state of both bone-forming and bone-fracturing processes with the predominance of one or another at different periods of life. This fact was reflected in their physical and mechanical characteristics. Thus, the values given in Tab. 2 are to be considered as approximate, while they could deviate noticeably in treatment of each individual patient.

Property	Cortical tissue	Trabecular tissue
Compressive strength, MPa	100–230	2–12
Bending and tensile strength, MPa	50–150	10–20
Elongation,%	1–3	5–7

Table 2: General data on the mechanical properties of bone tissue [32].

THE RESULTS OF COMPUTER SIMULATION

Calculated SSS for installed single implants

Initially, trial calculations of the SSS were carried out for installed single unconnected implants. In the upper position (top row), the only Zygan implant was fixed, while the only Oncology one was attached in the lower position (bottom row). Boundary conditions (4) and (5) were implemented. The $F^{(1)}$ load (Fig. 2, b) of 50 N was applied on the implant abutment vertically upward (along the Z axis).

Fig. 3 shows distributions of equivalent stresses and strains after the installation of the Zygan implant in the upper right position. Under the preset conditions, the zygomatic bones of the skull and the implant were characterized by a complex SSS. Due to the specific pattern of such fastening, the implant experienced predominantly bending strains when the vertical load was applied to its abutment. The fourth theory of strength (von Mises) was used, in which calculated values of equivalent stresses did not exceed critical levels of experimentally measured stresses for a material. Such equivalent stresses were assessed using the following formula:

$$\sigma_v = \sqrt{\frac{(\sigma_1-\sigma_2)^2+(\sigma_2-\sigma_3)^2+(\sigma_3-\sigma_1)^2}{2}} \le [\sigma]$$

where the yield stress value $[\sigma]$ for the Ti-6Al-4V alloy was applied as the critical level for the material under the calculations; σ_1, σ_2, σ_3 were principal stress tensor components. The critical SSS was observed when elastic strains were surpassed, but both plastic ones and the ultimate strength of bone tissue were achieved. Thus, the model employed Von Mises criteria for estimating the stress-strain state and reaching the critical state. The upper limit is related to their maximum values (being always positive), while their minimum values are equal to zero. The maximum and minimum data values are presented at the correspondent figures and tables.

The maximum level of σ_{eq} equivalent stresses of about 263 MPa was achieved in the titanium implant, in which the bending strain mode predominated. The maximum level of ε_{eq} equivalent strains of ~1.6% was observed at the interface between the implant and the zygomatic bone.

A more detailed view of the stress pattern in the zygomatic bone is shown in Fig. 3, c (without the implant for improving the presentation clarity). In this case, the σ_{eq} equivalent stress of 118 MPa was lower in the zygomatic bone than that in the implant. However, taking into account the considered mechanical properties of bone tissue (Tab. 1), this value generally exceeded the tensile strength, causing its failure. In (cortical) bone tissue, the maximum value of ε_{eq} equivalent stresses was ≥1.6%, which was also above the reported critical level, according to Tab. 1 [33,34].

The following result was noteworthy. Considering the applied load conditions, the implant displaced from bottom to top. Respectively, it was expected that the maximum stresses should take place in the upper part of the area of its attachment (Fig. 3, c). However, another pattern was found due to the given boundary conditions (adhesion at the "implant-bone tissue"

interface), as well as the area of the radial attachment of the implant to the zygomatic bone. Thus, it was shown that the pattern of the distributions of stresses and strains was determined not only by the bone tissue properties, but also by the implant attachment conditions.

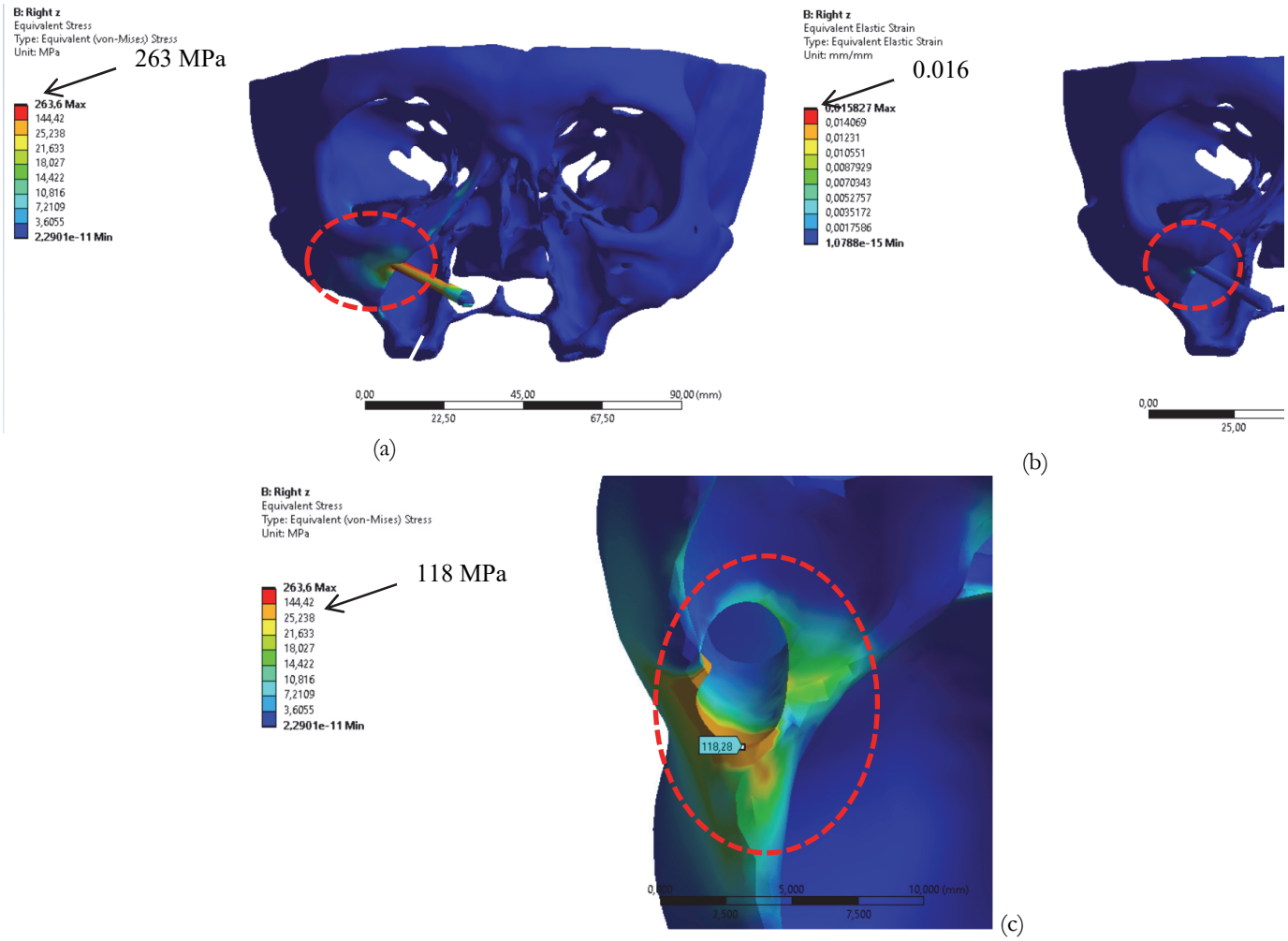

Figure 3: The distributions of equivalent stresses (a, c) and strains (b) at the installation of the Zygan implant in the upper right position; (a) general view; (c) stresses in bone tissue.

Since rising the load up to 100 and 150 N proportionally increased both stresses and strains, the results of such calculations are not presented. Similar parametric studies are reported below in Subsection 3.2 for the concentrated load applied to the implants through the denture base.

Fig. 4 shows distributions of equivalent stresses and strains after the installation of the Oncology implant in the lower right position. According to Fig. 4, a, the maximum σ_{eq} value of ~201 MPa was also observed at the interface between the implant and the zygomatic bone. Nevertheless, it was lower by ~60 MPa as compared to the previous case since the Oncology implant was shorter that the Zygan one. A more detailed view of the stress distribution, shown in Fig. 4, c, enabled to conclude that they did not exceed ~92 MPa in bone tissue. In the zygomatic bone, the maximum ε_{eq} values were within 1.3% (Fig. 4, b).

Fig. 5 shows distributions of equivalent stresses and strains at the installation of the Zygan implant in the upper left position. According to Fig. 5, a, the maximum σ_{eq} value of 244 MPa decreased by ~20 MPa compared to that for the right position at the "implant–zygomatic bone" interface. A more detailed view of the stress distribution pattern in the zygomatic bone (Fig. 5, c) showed that the maximum σ_{eq} value of ~96 MPa was lower than that for the right position. It should be noted that the maximum ε_{eq} stresses took place along the left side of the hole for installing the implant, but not in its upper part (Fig. 5, c). Similar to the case shown in Fig. 4, a, the reason for this phenomenon could be the large contact area between the implant and the zygomatic bone under the preset conditions of ideal adhesion. This fact indicated that the implant

configuration could give rise to significant redistribution of contact stresses. The maximum ε_{eq} values did not exceed 1.1% in bone tissue (Fig. 5, b), surpassing the reported critical elongation level [32].

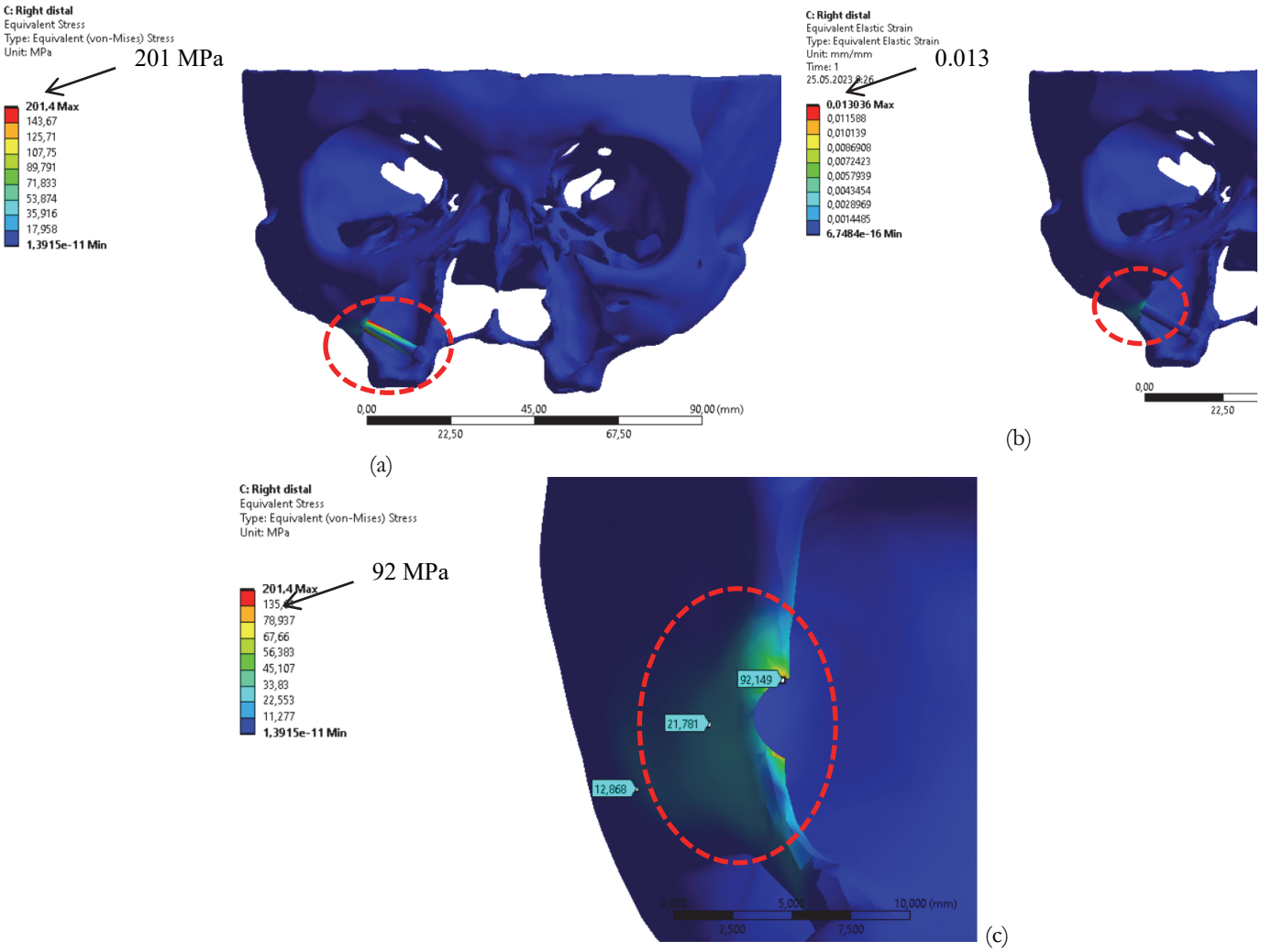

Figure 4: The distributions of equivalent stresses (a, c) and strains (b) at the installation of the Oncology implant in the lower right position; (a) general view; (c) stresses in bone tissue.

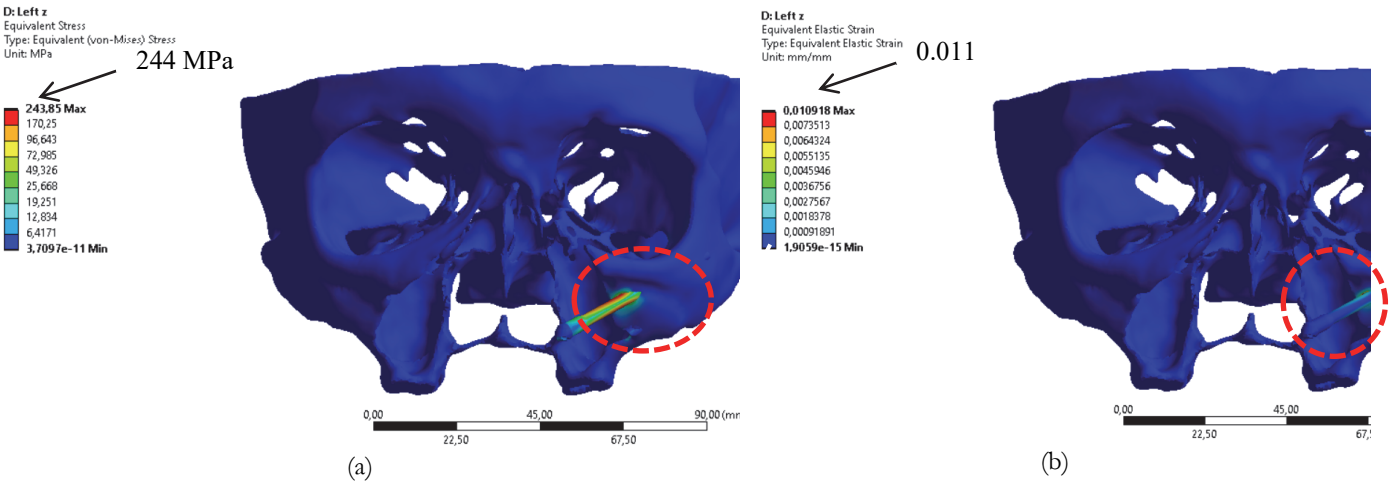

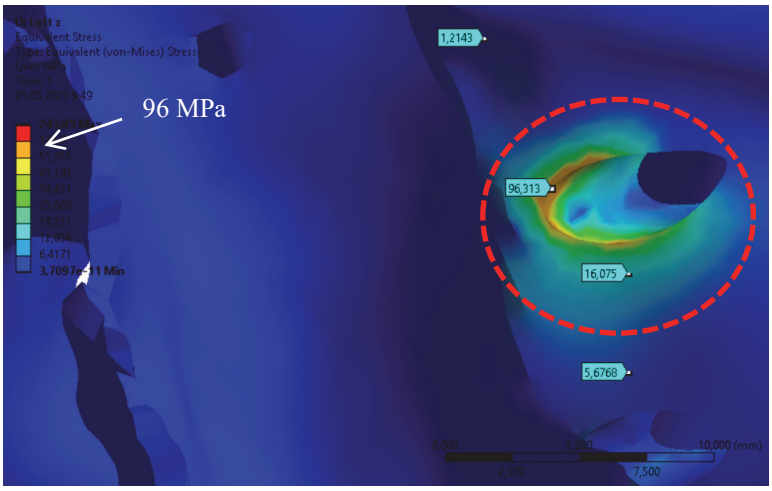

(c)

Figure 5: The distributions of equivalent stresses (a, c) and strains (b) at the installation of the Zygan implant in the upper left position; (a) general view; (c) stresses in bone tissue.

Fig. 6 presents distributions of equivalent stresses and strains at the installation of the Oncology implant in the lower left position. As in all the above-described cases, the maximum σ_{eq} value of 183 MPa was observed at the "implant–zygomatic bone" interface, which was lower by ~20 MPa than that for the right position according to Fig. 4. A more detailed view of the σ_{eq} distribution showed that their values did not exceed 128 MPa in the zygomatic bone, which was higher by ~30 MPa than that for the right position. According to Fig. 6, b, the ε_{eq} maximum values were within 1.4% in bone tissue (in contrast to ε_{eq}~1.3% for the Oncology implant shown in Fig. 4, b).

The maximum values of equivalent stresses and strains, determined in four performed calculations, are summarized in Tab. 3.

No.	Type and position of implant	Maximum equivalent stresses and strains		
		in structure, MPa	in zygomatic bone, MPa	in zygomatic bone, %
1	Zygan, the upper left position	263	118	1.6
2	Oncology, the lower right position	201	92	1.3
3	Zygan, the upper left position	244	90	1.1
4	Oncology, the lower left position	183	128	1.4

Table 3: The SSS parameters for the installed single zygomatic implants.

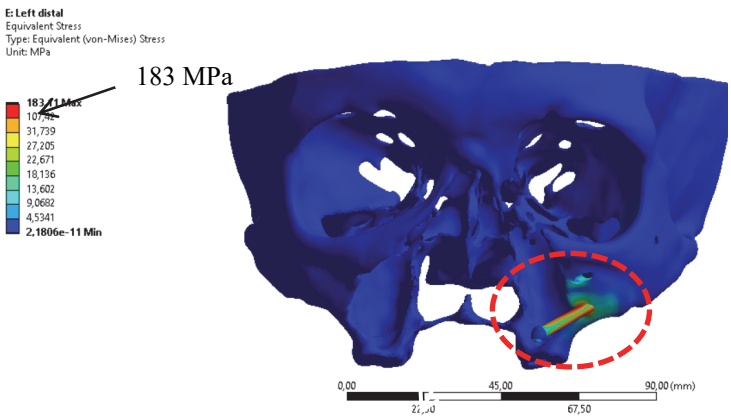

(a)

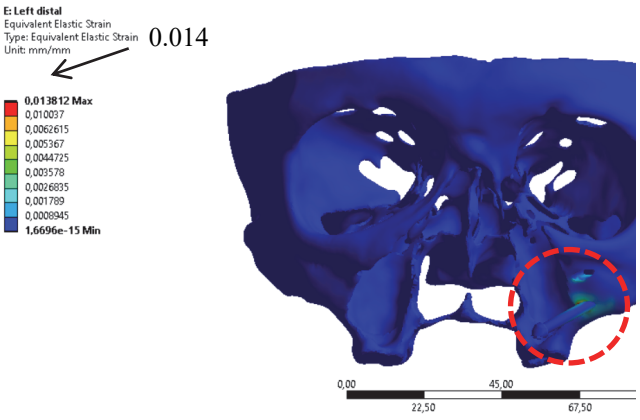

(b)

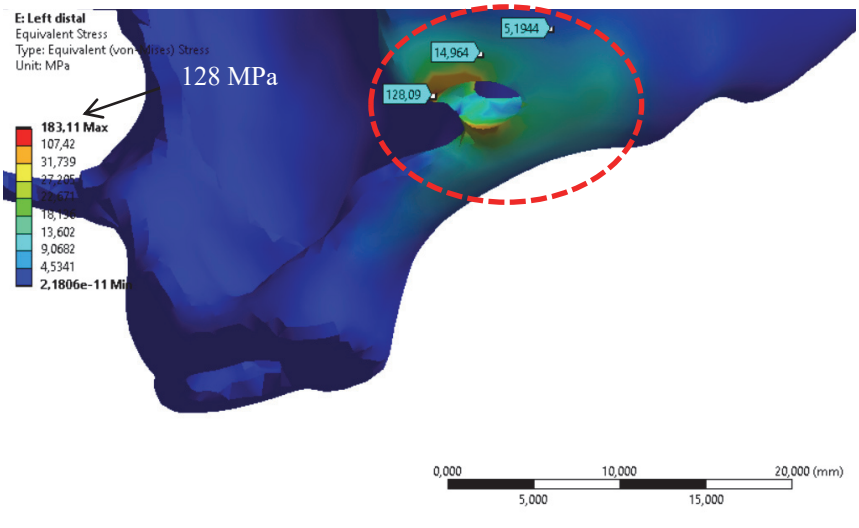

(c)

Figure 6: The distributions of equivalent stresses (a, c) and strains (b) at the installation of the Oncology implant in the lower left position; (a) general view; (c) stresses in bone tissue.

As a preliminary conclusion, two key identified results should be noted:
1) At concentrated loading of the implant, the distribution of stresses (and, accordingly, strains) was primarily determined by the implant length (through the arm size), as well as by the applied $F^{(1)}$ load of 50 N. After the multiple increase in the $F^{(1)}$ load up to 100 and 150 MPa, both stress and strain levels had to increase proportionally. Thus, if the fracture criterion was satisfied already at the minimum load, failure would inevitably occur at its average and maximum values.
2) The redistributions of both the patterns and the maximum stress levels depended on the macrostructure of the zygomatic bone (due to the resection of a fragment of bone tissue and fixation of the implant in its hole) and the mechanical properties. Since the "improved" digital model wad applied (as close as possible to the real structure), this fact enabled to explicitly consider the anatomical features of the structure of the zygomatic bones of the particular patient.
For this reason, the results of such trial calculations may be the basis for changing the attachment locations or the standard size of installed zygomatic implants (at the discretion of the maxillofacial surgeon). In addition, the CT data accuracy in terms of reproducing the structure of the zygomatic bone could be determined the effectiveness of the proposed approach for calculating the SSS and, accordingly, treatment tactics (including prosthetics).

Calculated SSS for installed all zygomatic implants and denture base

Since the ultimate goal of installing the implants was to attach the dentoalveolar prosthesis Fig. 1, c), the SSS calculations were carried out for the case of attachment the denture base (Fig. 1, d). For this purpose, the implant abutments were immovably fixed in the polymer denture base. In order to reduce the number of calculation elements, computer simulation was performed by alternating impact on the denture base segments (Fig. 2, c). It was divided into eight sequentially loaded segments (numbered from right to left, according to Fig. 2, c). Boundary conditions (4) and (6) were preset. The $F^{(2)}$ load was applied alternately to the segments in the direction orthogonal to the surface (Fig. 2, c). In this way, the biting off process was simulated. Three load levels of 50, 100 and 150 N were assumed. The load of 100 N corresponds to average mastication force, while the load of 150 N was employed to estimate the systems' performance under the overloading conditions. The SSS was assessed for the entire structure, including the zygomatic bones, the implants and the denture base. Tab. 4 presents the maximum values of equivalent von Mises stresses and strains for the entire (structure) system and separately for the zygomatic bones under different loading conditions. The calculated data are indicated for the most loaded both implants and areas of the zygomatic bones adjacent to the corresponding one. Through a slash, the values are given that were obtained by the calculation at the lower adhesion level (in contrast to the above data for ideal adhesion). This option could correspond to attachment of the implants to bone tissue with lower strength properties, for example. In most cases, a decrease in adhesion was accompanied by lowering the maximum local stresses. Nevertheless, other results were also observed when the location of the concentrator area changed, or the maximum stress level was higher than that for ideal adhesion.
Let us summarize, that two sets of computational experiments were carried out. The first one assumes low adhesion between the implants and bone tissue. In doing so, the area of rigid contact was incomplete being realized between the thread and cylindrical shape hole only. The boundary conditions at other contact sites of the zigomatic implant with the bone tissue

were set as sliding and separation. In the second case, the "rigid contact" boundary conditions were set over entire contact area between the implant and the bone, excluding any sliding. The first case was classified as the "low adhesion", while the "ideal adhesion" was postulated in the second case.

Loaded segment	*E*, GPa	In the model as a whole at (ideal/low) adhesion σ_{mis}, MPa	Concentrator location at (ideal/low) adhesion	In bone tissue at (ideal/low) adhesion		Concentrator location at (ideal/low) adhesion
				σ_{mis}, MPa	ε_{mis}, %	
1	50	156/130	LR / LR	52/39	0.52	LR / LR
	100	311/260		104/62	1.05	
	150	467/390		157/99	1.39	
2	50	86/188	LR / UR	41/31	0.42	LR / LR
	100	173/237		60/62	0.63	
	150	259/366		124/88	1.15	
3	50	91/122	UR / UR	33/29	0.33	LR / LL
	100	172/244		65/37	0.65	
	150	274/366		98/49	0.98	
4	50	88/98	UR / UR	40/39	0.4	LL / LL
	100	176/195		56/78	0.81	
	150	264/293		121/117	1.21	
5	50	65/70	UR / LL	41/36	0.41	LL / LL
	100	130/140		81/72	0.82	
	150	195/210		122/109	1.22	
6	50	50/67	LL / LU	27/23	0.27	LL / LL
	100	100/134		53/45	0.54	
	150	151/201		67/68	0.82	
7	50	53/61	LL / LU	41/28	0.44	LL / LL
	100	107/122		82/57	0.88	
	150	161/184		123/85	1.32	
8	50	149/101	LL / LL	60/39	0.64	LL / LL
	100	298/203		120/78	1.29	
	150	447/304		181/117	1.94	

σ_{mis} is equivalent stress, LR is lower right, LL is lower left, UR is upper right, UL is upper left.

Table 4: The calculated results under the action of the axial load on the segments of the denture base.

Fig. 7, a shows a histogram of the maximum σ_{eq} equivalent stresses in the model for the ideal adhesion case, depending on the number of the loaded segment at $F^{(2)}$=150 N, which indicated the location of the stress concentrator (according to the data in Tab. 4). Note that the maximum σ_{eq} values of 467 and 447 MPa were achieved when loading segments 1 and 8,

respectively. They were concentrated in the implants but their levels were not critical. With the yield strength of the Ti-6Al-4V alloy of 930 MPa, the safety factor was close to two that was acceptable to ensure the reliability of the titanium implant under the static loading. The minimum σ_{eq} values of 151 and 161 MPa were observed when loading segments 6 and 7, respectively.

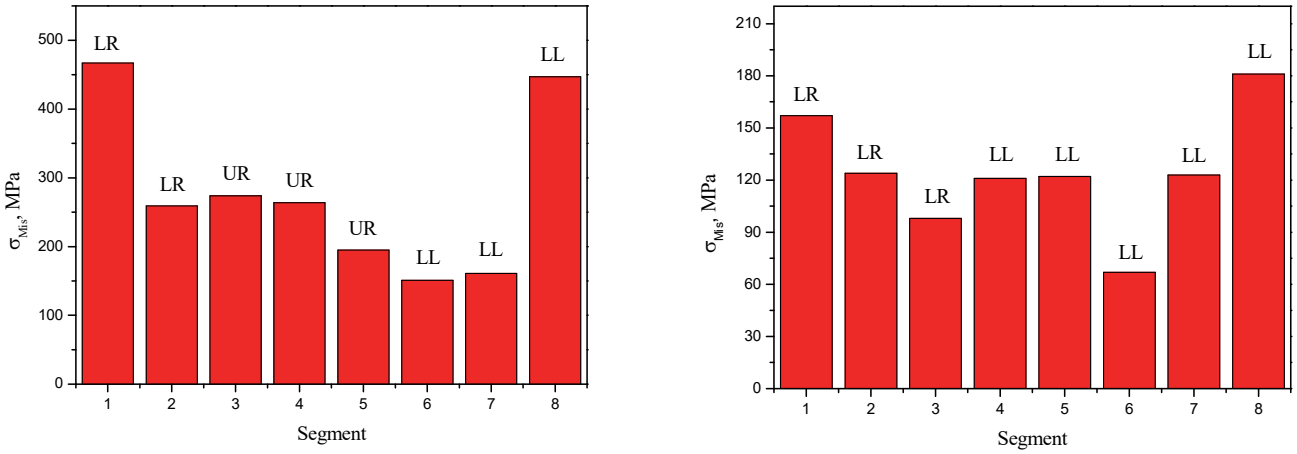

Figure 7: The histograms of the maximum values of equivalent stresses in the model as a whole (a) and in bone tissue (b) depending on the number of the loaded segment.

Regarding the distribution of equivalent stresses in bone tissue, it should be noted that the stress concentrator was found in the area of direct contact between the implant and the zygomatic bone. In accordance with the data presented in Tab. 4, a histogram of the maximum σ_{eq} values in the zygomatic bones is shown in Fig. 7,b, depending on the number of the loaded segment at $F^{(2)}$=150 N. The maximum σ_{eq} values of 157 and 181 MPa were observed in the zygomatic bones when loading segments 1 and 8, respectively, while the minimum ones of 98 and 67 MPa were characteristics when loading segments 3 and 6.

Fig. 8 shows distributions of equivalent stresses in the structure (system) as a whole (Fig. 8, a) and separately in the region of their concentration in bone tissue (Fig. 8, b) when loading segment 1 at $F^{(2)}$=150 N. The maximum σ_{eq} stresses of 157 MPa were concentrated at the main part of the implant (bending) and its lower right region (compressive).

In addition, Tab. 4 presents some more atypical results. In particular, the maximum σ_{eq} value of 264 MPa developed in the upper right part of the implant when the load was applied to segment 4 (which corresponded to the location of the right incisor), while the lower left part was maximally loaded in bone tissue, where equivalent stresses reached 121 MPa (Fig. 9, a). In this case, the region of maximum stress concentration in bone tissue are showed in Fig. 9, b. This result could be interpreted as follows. When the incisors were loaded in the maxillary prosthesis, "overturning" loads developed, redistributing stresses in the zygomatic bones and causing such an effect.

Another unexpected result presenting in Tab. 4 was the following. Given the external symmetry of the denture base and the identical standard size of the implants in the upper and lower attachments, the distribution of stresses in the implants was significantly different when loading segments 1–4 and 5–8. For example, the maximum σ_{eq} values were 467 and 447 MPa when loading a pair of segments 1 and 8, but they were 259 and 161 MPa for segments 2 and 7, 274 and 151 MPa for 3 and 6, as well as 264 and 195 MPa for 4 and 5, respectively. On the other hand, this difference was leveled out to a noticeable extent for bone tissue since equivalent stresses were 157 and 181 MPa when loading a pair of segments 1 and 8, 124 and 123 MPa for 2 and 7, 98 and 67 MPa for 3 and 6, as well as 121 and 122 MPa for 4 and 5, respectively. This fact reflected that the critical stresses were reached in bone tissue not only when the load was applied to the anterior block of teeth, which was less resistant to vertical loads (namely, the incisors).

Fig. 10 shows the displacement fields for loaded segments 1 and 8 at $F^{(2)}$=150 N. As was noted above, the maximum stress levels were observed in both the implants and the zygomatic bones under these loading conditions. Accordingly, the maximum displacements took place in the model as well. In the case of loading segment 1 (Fig. 10, a c), the displacement of the prosthetic structure of 0.880 mm was much higher (up to eight times) than that (0.104 mm) in the lower right area of the zygomatic bone near the implant. When segment 8 was loaded (Fig. 10, b d), the displacement of the prosthetic structure of 1.112 mm was greater by twelve times than that (0.091 mm) in the lower left part of the zygomatic bone. In both cases,

the difference between the maximum displacements was about 10%. The absence of a fragment of bone tissue in the area of the junction of the zygomatic bone with the bridge of the nose qualitatively affected the pattern of the displacement redistributions, but to a much lesser extent for the obtained quantitative values.

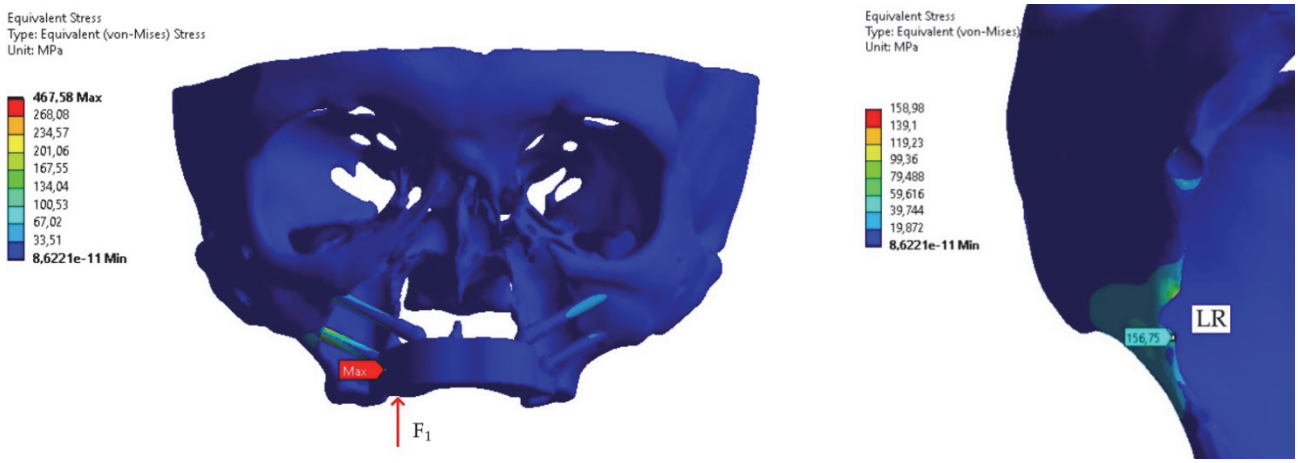

a) b)

Figure 8: The distributions of equivalent stresses in the structure at the $F^{(2)}$ load of 150 N applied on segment 1: a) stresses in the structure; b) the maximum stress in bone tissue.

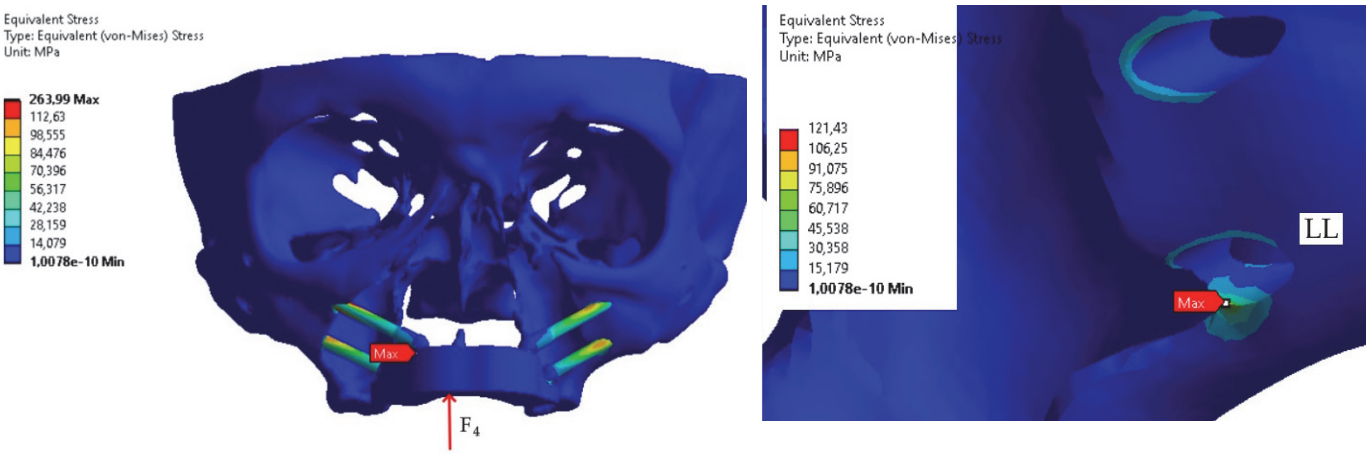

a) b)

Figure 9: The distributions of equivalent stresses in the structure at the $F^{(2)}$ load of 150 N applied on segment 4: a) stresses in the system; b) the maximum stress in bone tissue.

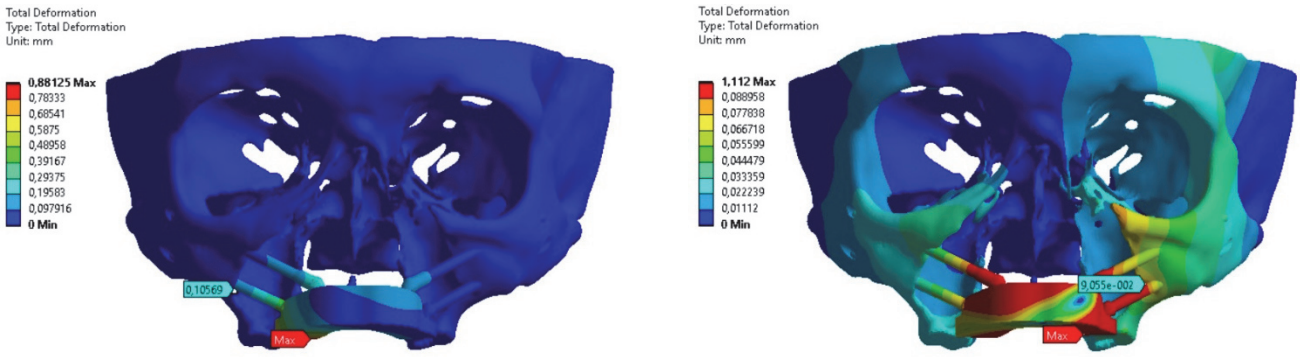

a) b)

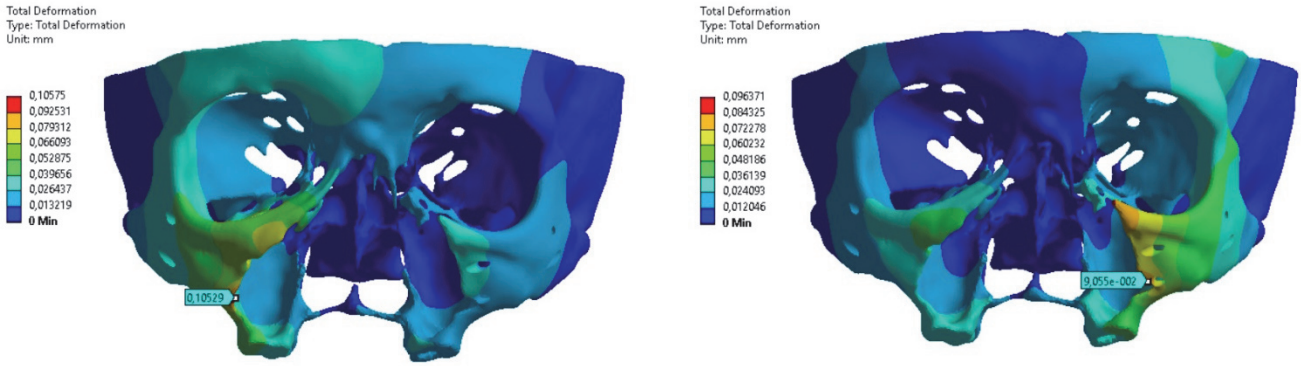

c) d)

Figure 10: The distributions of total displacements of the system and bone tissue at the $F^{(2)}$ load of 150 N applied on segments 1 (a, c) and 8 (b, d).

It should be noted as a discussion point that bone tissue adapts to applied loads according to Wolff's law. Respectively, this phenomenon controls the remodeling process and, as a consequence, the resulting quality and architecture. Thus, the response of the zygomatic bones depends on the magnitude of the applied load in addition to controlling the level of critical stresses/strains (determining the likelihood of failure). If the level of developing stresses is within the physiological range of about 20–60 MPa, the bone tissue remodeling occurs, but pathological microfractures and necrosis may be observed in other cases [35-39]. In addition, the mechanical response of bone tissue around implants also depends on the direction and magnitude of the applied load, as well as the quantity/quality of both bones and implants (design, material, production routs, etc.) [40-42].

Calculated SSS for all installed zygomatic implants and denture base under non-axial loads

During mastication, different groups of teeth experience various loads not only in their levels, but also in the direction of their application. Thus, if molars and premolars predominantly operate in the food grinding mode, when the load direction predominantly coincides with the vertical axis of the tooth, then the anterior blocks of teeth (incisors and canines) predominantly operate in the biting off mode, when the "angle of attack" can differ markedly from normal. For this reason, the SSS calculation was carried out for the case of non-axial loading the anterior block of teeth. Boundary conditions (4) and (7) were preset, respectively. The $F^{(3)}$ load was applied alternately to segments 4 and 5 at the angle of 45° (Fig. 2, c). Similar to problem 2, three $F^{(3)}$ load levels of 50, 100 and 150 N were taken in the calculations. The SSS of the entire system, including the zygomatic bones and the implants, was assessed.

Data of the maximum values of equivalent stresses and von Mises strains for the entire system are summarized in Tab. 5 in addition to those for the zygomatic bones under various non-axial loading conditions. The calculated data are indicated for the most loaded both implants and areas of the zygomatic bones adjacent to the corresponding ones.

Fig. 11 shows distributions of stresses after applying the $F^{(3)}$ load of 150 N on segment 4 at the angle of 45°. Regions of the maximum stresses are outlined with ovals in Fig. 12, a for the system and in Fig. 12, b for bone tissue, respectively. In the case of non-axial loading the anterior segments, the SSS changed qualitatively and quantitatively, both in the structure (system) as a whole and in the zygomatic bones separately.

After applying the $F^{(3)}$ load of 150 N on segment 4 in the orthogonal direction, the maximum equivalent stresses of 267 MPa were found in the lower right implant, but they were 264 MPa in the upper right one.

The zygomatic bones showed a similar pattern, i.e. the stress concentration was in the lower left region, but the maximum value of 201 MPa was twice that under the orthogonal load, causing an increase in the σ_{eq} values of up to 2.2% in this region that could result in fast failure at this load level. When loading segment 5 as well as segments 4 and 5 simultaneously, the maximum levels of equivalent stresses of 265 and 240 MPa were achieved in the left lower implant, but they were 246 and 223 MPa in the zygomatic bone and in the lower left region near the implant, respectively. At the same time, equivalent strains of bone tissue were 2.46 and 2.23%, respectively, exceeding the critical level. Note that they were higher than those under orthogonal loading. It could be concluded that non-axial loading the anterior segments (in the biting off mode) led to greater stresses and strains. In addition, a redistribution of the load between the implants could occur in the case of loading segment 4.

No.	Loaded segment	F_i, N	Maximum equivalent stresses and strains		
			in the system, MPa	in zygomatic bone, MPa	in zygomatic bone, %
1	4	50	89	67	0.67
		100	178	134	1.34
		150	267 (LR)	201 (LL)	2.02
2	5	50	88	82	0.82
		100	177	164	1.64
		150	265 (LL)	246 (LL)	2.46
3	4 and 5 simultaneously	50	80	74	0.74
		100	160	148	1.48
		150	240 (LL)	223 (LL)	2.23

F_i is a load on segment

Table 5: The calculated results for the non-axial loads on the anterior segments of the denture base.

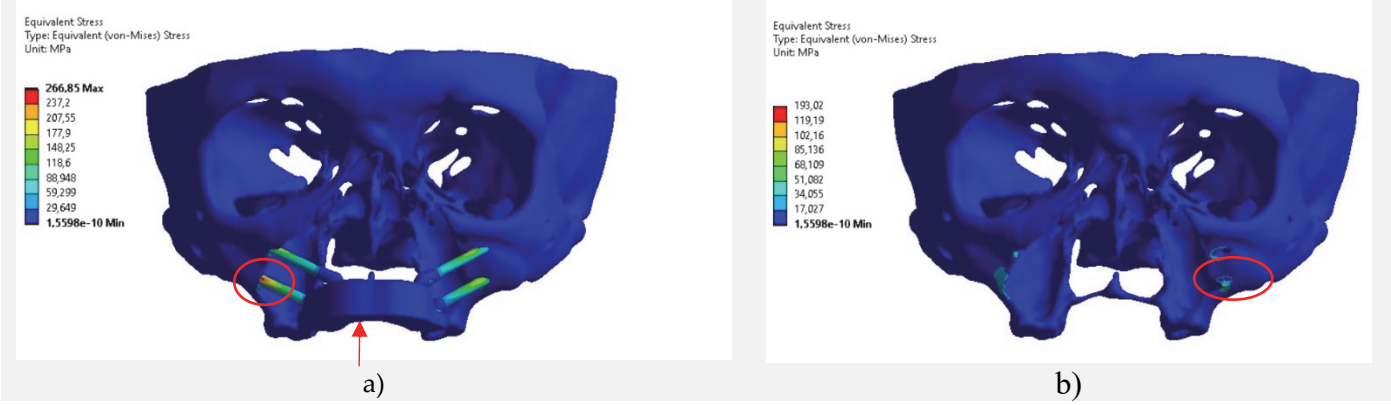

Figure 11: The distributions of equivalent stresses at the $F^{(3)}$ non-axial load of 150 N applied on segment 5: a) in the system; b) in bone tissue.

Figure 12 shows the displacement fields in the model after loading segment 4 both in the orthogonal direction and at the angle of 45°. The maximum displacement value of 0.95 mm was observed for the non-axial loading conditions, but it was only 0.62 µm in the second case. In addition, displacements of the zygomatic bones reached greater values of 0.112 mm (right) and 0.122 mm (left) in the first case, but they were 0.083 and 0.078 mm, respectively, for the second loading mode.

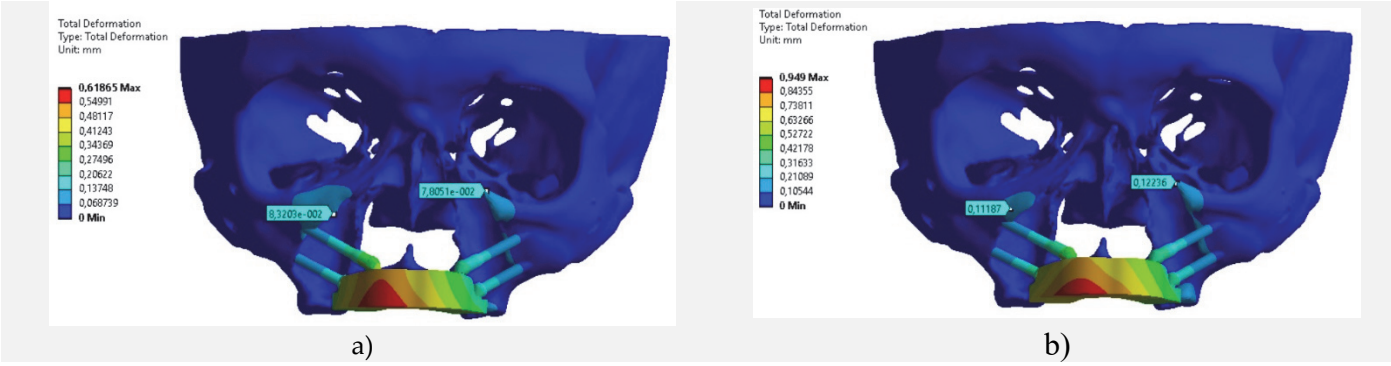

Figure 12: The distributions of the displacements in the model at the $F^{(3)}$ non-axial load of 150 N applied on segment 4: a) orthogonal loading; b) non-axial loading.

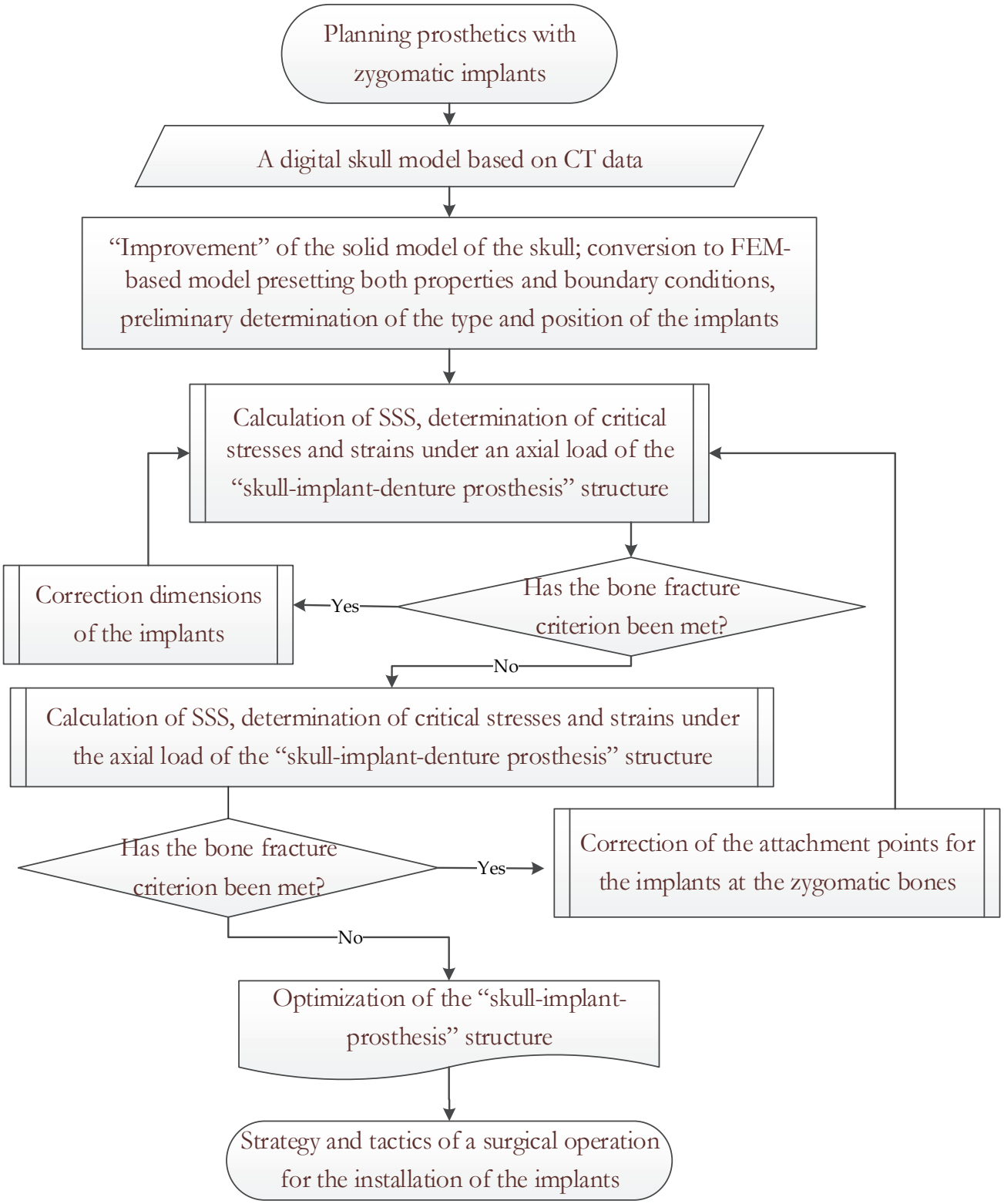

Figure 13: The algorithm of the FEM-based computer simulation for planning prosthetics with zygomatic implants.

Discussion

The first important result of the study should be considered the revealed fact that the response of the "skull-zygomatic implant-denture base" system was not always linear, despite the SSS calculations were carried out in the elastic statement. The reasons were the following factors.

- In the model of the skull, the attachment points of the implants could not be identical everywhere (including the contact area between the implant and bone tissue) due to the anatomical features.
- The calculated results depended on the adhesion conditions at the interface between the implants and bone tissue.
- When the load was applied to individual segments, the redistribution of stresses and strains took place.
- There was obvious macroscopic heterogeneity of the developed model (first of all, a disconnection of the zygomatic bone with the bridge of the nose).

As noted above, an additional factor could be the heterogeneity of both properties of bone tissue and its thickness in various regions.

The authors considered it important to focus attention on the result obtained by varying the adhesion conditions at the "implant-zygomatic bone" interface (Subsection 3.2). It was shown that lowering the adhesive strength at the area of implants-to-bone-issue attachment was accompanied by the slight decrease in both stresses and strains. In some cases, this phenomenon was accompanied by achieving the critical stress level. In addition, the overload location could differ from the calculated results in the ideal adhesion case. This fact possessed a double meaning. On the one hand, it could be considered as a case of attachment of the implant to the zygomatic bone with lower density and, accordingly, less retention ability. In addition, it could correspond to another case of low osseointegration of the implant. On the other hand, it was shown that high levels and even critical stresses could develop in the zygomatic bones. From the point of view of the SSS calculation using the applied model, this fact indicated that the more significant factor was the implant action as a clamped beam (but not the adhesion level) according to the strength of materials. Noted that the obtained data were not absolutely accurate due to the applied approximation. In addition, the results characterized by a certain subjectivity after "improving" the digital model of the skull, removing a number of artifacts, and choosing the computational mesh parameters. However, the proposed approach can be used to solve some practically important problems of complex maxillofacial treatment within the predictive accuracy limits. Since the FEM-based computer simulation was not the only purpose of this research, the authors proposed an algorithm for planning prosthetics with zygomatic implants (Fig. 13).

Conclusions

For the FEM-based computer simulation, the digital model of the "skull-zygomatic implants-denture base" structure (system) was developed. Its implementation in the computational experiments enabled to calculate the SSS of the structure loaded on individual segments and the whole system. The efficiency of the installation of the zygomatic implants was assessed according to the fracture/critical state criterion (tensile strength/deformation due to failure of bone tissue). The obtained results made it possible to draw the following conclusions:

1. At the load of 150 N, stresses could develop in the zygomatic bones that exceeded their tensile strength, while various positions of the implants were characterized by fundamentally different stress levels. In most cases, their maximum values were observed in the low left region of the zygomatic bones, reaching the critical level (the fracture criterion was met). At the orthogonal load of 100 N on segment 8, the maximum stresses reached 120 MPa in the zygomatic bones, which could be considered as fulfillment of the fracture criterion as well. Changing the adhesion conditions at the "zygomatic implant–bone tissue" interface varied both the level of maximum stress and the location of the critical stress concentrator.
2. The local load applied on different segments of the denture base could cause the formation of a critical concentrator due to the redistribution of stresses at the area of attachment of the zygomatic implant to bone tissue.
3. The local disturbance of the integrity of bone tissue in the skull was one of the key reasons for the redistribution of stresses in the "skull-zygomatic implant-denture base" system. Such a phenomenon should be primarily taken into account when choosing the standard sizes of installed zygomatic implants in order to reduce the compliance of weakened areas of the skull (as the basis of the load-bearing structure).
4. Lowering the adhesive strength in the area of attachment of the zygomatic implants in bone tissue was accompanied by reducing both stresses and strains, but could not avoid the achievement of the critical stress level. In this case, the stress concentrator location could differ from that under the ideal adhesion conditions since the pattern of the SSS was primarily determined by the implant action as a clamped beam.

5. Based on the results of the FEM-based computer simulation, the algorithm was proposed for planning prosthetic treatment, which involves the iterative method for selecting both size and location of attachment of zygomatic implants depending on the results of the SSS calculation and the onset of a critical condition (primarily in bone tissue at the area of attachment of zygomatic implants).

ACKNOWLEDGEMENT

Sergey Panin acknowledges support from the project FWRW-2021-0010 through the government research assignment for ISPMS SB RAS.

REFERENCES

[1] Kaprin, A.D., Starinskij, V.V., Petrova, G.V. (2019). Zlokachestvennye novoobrazovaniya v Rossii v 2018 godu (zabolevaemost' i smertnost'). M.: MNIOI im. P.A. Gercena — filial FGBU «NMIC radiologii» Minzdrava Rossii. (In Russ.).

[2] WHO. Cancer Newsletter. Geneva: WHO; (2018). Accessed September 8, 2020. https://gco.iarc.fr/today/data/factsheets/populations/900-world-fact-sheets.pdf

[3] Kofler, B., Laban, S., Busch, C.J., Lörincz, B., Knecht R. (2013), New treatment strategies for HPV-positive head and neck cancer. European Archives of Oto-Rhino-Laryngology, 271(7), pp. 1861-1867. DOI: 10.1007/s00405-013-2603-0.

[4] Brånemark, P., Gröndahl, K., Öhrnell, L., Nilsson, P., Petruson, B., Svensson, B., Nannmark, U. (2004). Zygoma fixture in the management of advanced atrophy of the maxilla: technique and long-term results. Scandinavian Journal of Plastic and Reconstructive Surgery and Hand Surgery, 38(2), 70–85. DOI: 10.1080/02844310310023918.

[5] Aparicio, C., Manresa, C., Francisco, K., Claros, P., Alández, J., González-Martín, O. and Albrektsson, T. (2014). Zygomatic implants: indications, techniques and outcomes, and the Zygomatic Success Code, Periodontology 2000, 66(1), pp. 41–58. DOI: 10.1111/prd.12038.

[6] Polido, W.D., Machado-Fernandez, A., Lin, W.S., Aghaloo, T. (2023). Indications for zygomatic implants: a systematic review. Int J Implant Dent.,9(1), 17. DOI: 10.1186/s40729-023-00480-4.

[7] Solà Pérez, A., Pastorino, D., Aparicio, C., Pegueroles Neyra, M., Khan, R.S., Wright, S., Ucer, C. (2022). Success Rates of Zygomatic Implants for the Rehabilitation of Severely Atrophic Maxilla: A Systematic Review, Dent J (Basel), 10(8), 151. DOI: 10.3390/dj10080151.

[8] Migliorança, R.M., Coppedê, A., Dias Rezende, R.C., de Mayo, T. (2011). Restoration of the edentulous maxilla using extrasinus zygomatic implants combined with anterior conventional implants: a retrospective study. Int J Oral Maxillofac Implants. 26(3), pp. 665-672.

[9] Vrielinck, L., Blok, J., Politis, C. (2022). Survival of conventional dental implants in the edentulous atrophic maxilla in combination with zygomatic implants: a 20-year retrospective study. Int J Implant Dent., 8(1), 27. DOI: 10.1186/s40729-022-00425-3.

[10] Bidez, M. W. and Misch, C. E. (1992). Issues in bone mechanics related to oral implants. Implant Dentistry, 1(4), pp. 289–294. DOI: 10.1097/00008505-199200140-00011.

[11] Bedrossian, E., Bedrossian, E.A. (2019). Fundamental principles for immediate implant stability and loading. Compendium, 40(9), pp. 1–8. https://www.straumann.com/content/dam/media-center/straumann/en-us/documents/case-study/Fundamental-principals-Bedrossian-BLX-immediacy-case-study.pdf

[12] Candel-Martí, E., Carrillo-García, C., Peñarrocha-Oltra, D., Peñarrocha-Diago, M. (2012). Rehabilitation of atrophic posterior maxilla with zygomatic implants: review. J Oral Implantol., 38(5), 653-657. DOI: 10.1563/AAID-JOI-D-10-00126.

[13] Aparicio, C., López-Piriz, R. and Albrektsson, T. (2020). ORIS Criteria of Success for the Zygoma-Related Rehabilitation: The (Revisited) Zygoma Success Code. The International Journal of Oral & Maxillofacial Implants, 35(2), pp. 366–378. DOI: 10.11607/jomi.7488.

[14] Ishak, M.I., Abdul Kadir, M.R., Sulaiman, E., Abu Kasim, N.H. (2012). Int J Oral Maxillofac Surg. 41(9), 1077-1089. DOI: 10.1016/j.ijom.2012.04.010.

[15] Wen, H., Guo, W., Liang, R., Xiang, L., Long, G., Wang, T., Deng, M., Tian, W. (2014). Finite element analysis of three zygomatic implant techniques for the severely atrophic edentulous maxilla. J Prosthet Dent., 111(3), 203-215. DOI: 10.1016/j.prosdent.2013.05.004.

[16] Romeed, S.A., Hays, R.N., Malik, R., Dunne, S.M. (2015). Extrasinus zygomatic implant placement in the rehabilitation of the atrophic maxilla: three-dimensional finite element stress analysis. J Oral Implantol., 41(2), pp. e1-6. DOI: 10.1563/AAID-JOI-D-12-00276.

[17] Ishak, M. I., Kadir, M. R. A., Sulaiman, E. and Kasim, N. H. A. (2013). Finite Element Analysis of Zygomatic Implants in Intrasinus and Extramaxillary Approaches for Prosthetic Rehabilitation in Severely Atrophic Maxillae. The International Journal of Oral & Maxillofacial Implants, 28(3), pp. e151–e160. DOI: 10.11607/jomi.2304.

[18] Zhenhuan, W., Yu, D., Junsi, L., Xiaowei, J., Zongyu, X., Li, L. (2020). Physiochemical and biological evaluation of SLM-manufactured Ti-10Ta-2Nb-2Zr alloy for biomedical implant applications. Biomed Mater, 15. DOI: 10.1088/1748-605X/ab7ff4.

[19] Omidi, S., Bahmani Oskooee, M. (2013). Analysis of stress concentration in bone–implant interface using different shapes of the implant: Porous Ti and ultra-fine grained Ti. Indian J Dent, 4, 125–128. DOI: 10.1016/j.ijd.2013.07.008.

[20] Macedo, J.P., Pereira, J., Faria, J., Souza, J.C.M., Alves, J.L., Lopez-Lopez, J. (2018). Finite element analysis of peri-implant bone volume affected by stresses around Morse taper implants: effects of implant positioning to the bone crest. Comput Methods Biomech Biomed Engin., 21, pp. 655–662. DOI: 10.1080/10255842.2018.1507025.

[21] Grachev, D.I., Ruzuddinov, N.S., Arutyunov, A.S., Akhmedov, G.D., Dubova, L.V., Kharakh, Y.N., Panin, S.V., Arutyunov, S.D. (2022). Algorithm for Designing a Removable Complete Denture (RCD) Based on the FEM Analysis of Its Service Life. Materials, 15, 7246. DOI: 10.3390/ma15207246.

[22] Souza, V., Matsuda, R., Peres, A., Amorim, P., Moraes, T., Silva, J., Baffa, O. (2019). In Vesalius Navigator, a free and open-source software for navigated transcranial magnetic stimulation, Brain Stimulation, 12(2), 571, DOI: 10.1016/j.brs.2018.12.894.

[23] Perevalova, O.B., Panin, A.V., Kazachenok, M.S., Sinyakova, E.A. (2022). Effect of Ultrasonic Impact Treatment on Structural Phase Transformations in Ti-6Al-4V Titanium Alloy. Phys. Mesomech., 25(3), 248. DOI: 10.1134/S1029959922030055.

[24] Zhang, W., Mehrabian, A. (2023). Coupled Poromechanics and Adsorption in Multiple-Porosity Solids. Phys. Mesomech., 26(4), pp. 402-414. DOI: 10.1134/S1029959923040033.

[25] Gupta, Y., Iyer, R., Dommeti, V.K., Nutu, E., Rana, M., Merdji, A. (2021). Design of dental implant using design of experiment and topology optimization: a finite element analysis study. Proc Inst Mech Eng Part H, J Eng Med., 235, pp. 157–166. DOI: 10.1177/0954411920967146.

[26] Huang, R., Liu, L., Li, B., Qin, L., Huang, L., Yeung, K.W.K. (2021). Nanograins on Ti-25Nb-3Mo-2Sn-3Zr alloy facilitate fabricating biological surface through dual-ion implantation to concurrently modulate the osteogenic functions of mesenchymal stem cells and kill bacteria. J Mater Sci Technol., 73, pp. 31–44. DOI: 10.1016/j.jmst.2020.07.048.

[27] Tretto, P.H.W., Dos Santos, M.B.F., Spazzin, A.O., Pereira, G.K.R., Bacchi, A. (2020). Assessment of stress/strain in dental implants and abutments of alternative materials compared to conventional titanium alloy-3D non-linear finite element analysis. Comput Methods Biomech Biomed Engin., 23, pp. 372–383. DOI: 10.1080/10255842.2020.1731481.

[28] Robau-Porrua, A., Perez-Rodríguez, Y., Soris-Rodríguez, L.M., Perez-Acosta, O., Gonzalez, J.E. (2021). The effect of diameter, length and elastic modulus of a dental implant on stress and strain levels in peri-implant bone: a 3D finite element analysis. Biomed Mater Eng, 30, pp. 541–558. DOI: 10.3233/BME-191073.

[29] Dias Corpa Tardelli, J., Lima da Costa Valente, M., Theodoro de Oliveira, T., Candido, dos Reis, A. (2021). Influence of chemical composition on cell viability on titanium surfaces: a systematic review. J Prosthet Dent., 125, pp. 421–425. DOI: 10.1016/j.prosdent.2020.02.001.

[30] Dias Corpa Tardelli, J., Bolfarini, C., Candido Dos Reis, A. (2020). Comparative analysis of corrosion resistance between beta titanium and Ti-6Al-4V alloys: A systematic review. J Trace Elem Med Biol Organ Soc Min Trace Elem, 62, 126618. DOI: 10.1016/j.jtemb.2020.126618.

[31] Grachev, D.I., Chizhmakov, E.A., Stepanov, D.Y., Buslovich, D.G., Khulaev, I.V., Deshev, A.V., Kirakosyan, L.G., Arutyunov, A.S., Kardanova, S.Y., Panin, K.S., Panin, S.V. (2023). Dental Material Selection for the Additive Manufacturing of Removable Complete Dentures (RCD). Int J Mol Sci., 24(7), 6432. DOI: 10.3390/ijms24076432.

[32] Milazzo, M., Contessi Negrini, N., Scialla, S., Marelli, B., Farè, S., Danti, S., Buehler, M.J. (2019). Additive Manufacturing Approaches for Hydroxyapatite-Rein load Composites. Adv. Funct. Mater., 29, 1903055. DOI: 10.1002/adfm.201903055.

[33] Grzeszczak, A., Lewin, S., Eriksson, O., Kreuger, J., Persson, C. (2021). The Potential of Stereolithography for 3D Printing of Synthetic TrabecularBone Structures. Materials, 14, 3712. DOI: 10.3390/ma14133712.

[34] Barak, M.M., Black, M.A. (2018). A novel use of 3D printing model demonstrates the effects of deteriorated trabecular bone structure on bone stiffness and strength. J. Mech. Behav. Biomed. Mater., 78, pp. 455–464. DOI: 10.1016/j.jmbbm.2017.12.010.

[35] Piotrowski, B., Baptista, A.A., Patoor, E., Bravetti, P., Eberhardt, A., Laheurte, P. (2014). Interaction of bone-dental implant with new ultra low modulus alloy using a numerical approach. Mater Sci Eng C Mater Biol Appl., 38, pp. 151–60. DOI: 10.1016/j.msec.2014.01.048.

[36] Liu, B., Xu, W., Chen, M., Chen, D., Sun, G., Zhang, C. (2022). Structural design and finite element simulation analysis of grade 3 graded porous titanium implant. Int J Mol Sci., 23, 10090. DOI: 10.3390/ijms231710090.

[37] Sun, J., Xiong, Y., Li, Y., Sun, F., Zhang, F. (2011). Structural optimization and three-dimensional finite element analysis of functionally graded dental implants. J Clin Rehabil Tissue Eng Res., 15, 8960–8963. DOI: 10.3969/j.issn.1673-8225.2011.48.008.

[38] Ausiello, P., Tribst, J.P.M., Ventre, M., Salvati, E., di Lauro, A.E., Martorelli, M. (2021). The role of cortical zone level and prosthetic platform angle in dental implant mechanical response: a 3D finite element analysis. Dent Mater., 37, pp. 1688–97. DOI: 10.1016/j.dental.2021.08.022.

[39] Li, J., Jansen, J.A., Walboomers, X.F., van den Beucken, J.J. (2020). Mechanical aspects of dental implants and osseointegration: a narrative review. J Mech Behav Biomed Mater., 103, 103574. DOI: 10.1016/j.jmbbm.2019.103574.

[40] Akbarinia, S., Sadrnezhaad, S.K., Hosseini, S.A. (2020). Porous shape memory dental implant by reactive sintering of TiH2–Ni-Urea mixture. Mater Sci Eng C., 107, 110213. DOI: 10.1016/j.msec.2019.110213.

[41] Tardelli, J.D.C., da Costa Valente, M.L., Macedo, A.P., dos Reis, A.C. (2022). Evaluation of biomechanical and stress distribution of different dental implant designs: primary stability and photoelastic analysis. IRBM., 43, pp. 100–106. DOI: 10.1016/j.irbm.2021.01.003.

[42] Spies, B.C., Bateli, M., Ben Rahal, G., Christmann, M., Vach, K., Kohal, R.J. (2018). Does oral implant design affect marginal bone loss? Results of a parallel-group randomized controlled equivalence trial. BioMed Res Int, 8436437. DOI: 10 .1155 / 2018 /8436437.